An Adaptive Fault-Tolerant Sliding Mode Control Allocation Scheme for Multirotor Helicopter Subject to Simultaneous Actuator Faults

Ban Wang, and Youmin Zhang, *Senior Member*, *IEEE*

***Abstract*—This paper proposes a novel adaptive sliding mode based control allocation scheme for accommodating simultaneous actuator faults. The proposed control scheme includes two separate control modules with virtual control part and control allocation part, respectively. As a low-level control module, the control allocation/re-allocation scheme is used to distribute/redistribute virtual control signals among the available actuators under fault-free or faulty cases, respectively. In the case of simultaneous actuator faults, the control allocation and re-allocation module may fail to meet the required virtual control signal which will degrade the overall system stability. The proposed online adaptive scheme can seamlessly adjust the control gains for the high-level sliding mode control module and reconfigure the distribution of control signals to eliminate the effect of the virtual control error and maintain stability of the closed-loop system. In addition, with the help of the boundary layer for constructing the adaptation law, the overestimation of control gains is avoided, and the adaptation ceases once the sliding variable is within the boundary layer. A significant feature of this study is that the stability of the closed-loop system is guaranteed theoretically in the presence of simultaneous actuator faults. The effectiveness of the proposed control scheme is demonstrated by experimental results based on a modified unmanned multirotor helicopter under both single and simultaneous actuator faults conditions with comparison to a conventional sliding mode controller and a linear quadratic regulator scheme.**

***Index Terms*—Adaptive sliding mode control, control allocation/re-allocation, fault-tolerant control, hardware redundancy, multirotor helicopter, simultaneous actuator faults.**

I. Introduction

With the increasing demands for unmanned aerial vehicles (UAVs) in both military and civilian applications, such as border surveillance, forest fire detection, and power-line inspection, critical safety issues should be considered significantly in order to make better and wider uses of them. In order to accomplish a specific mission, different sensors and measurement systems are incorporated with a UAV to make it become a fully functional system, which is often referred to as an unmanned aerial system (UAS). In this regard, a UAV can be treated as a sensor carrier, and usually the cost of those on-board instruments can easily exceed the cost of the UAV itself. Therefore, the reliability and survivability of UAVs are becoming the paramount concerns. Especially, for those applications carried out in urban areas, any failure occurred in a UAV may easily damage the UAV and its surroundings including the safety of the operators. Hence, it will be beneficial to have a UAV system with the capability of tolerating certain faults and even failures without imperiling itself and its surroundings. Here, a fault implies a partial loss of actuator control effectiveness, while a failure states a complete loss of actuator control effectiveness. As argued in [1], [2] and [3], the increasing demands for safety, reliability, and high system performance have stimulated research in the area of fault-tolerant control (FTC) with the development in control theory and computer technology. Fault-tolerant capability is an important feature for safety-critical systems [3], such as UAVs [4], spacecrafts [5], wind turbines [6], [7] etc., which will help to minimize the effect of possible faults/failures in the system and preserve the performance of the entire system.

Among those different types of UAVs, multirotor helicopters draw more and more attention in both industrial and academic communities due to their simplicity and affordable price. As an example of multirotor helicopters, a quadrotor helicopter is a relatively simple and easy-to-fly system. Thus, it has been widely used to develop and test methodologies in flight control [8], [9], multi-agent cooperative control [10], [11], and fault detection and diagnosis (FDD) and fault-tolerant control [12]–[14]. In terms of developing and testing advanced FDD and FTC schemes on quadrotor helicopters, the work described in [4] represents the cutting edge research in this area. However, due to the configuration of quadrotor helicopter, it lacks available actuator redundancy which is critical for a safer operation. As a consequence, a failure of any one of the motors will result in a crash of the quadrotor helicopter. In this case, it will harm not only the UAV itself but also its surroundings, which is catastrophic especially for those applications carried out in urban areas. For this reason, FTC should be considered and embedded in flight control laws for UAVs to improve the reliability and safety of UAV systems. Most studies about FTC on quadrotor helicopters only consider partial actuator fault in the literature due to the

Manuscript received April 14, 2017; revised August 6, 2017 and September 27, 2017; accepted October 14, 2017. This work was supported in part by the scholarships from China Scholarship Council (CSC) (No. 201406290023) and Natural Sciences and Engineering Research Council of Canada (NSERC).

B. Wang and Y. M. Zhang (Corresponding Author) are with the Department of Mechanical, Industrial & Aerospace Engineering, Concordia University, Montreal, Canada (e-mail: ban_w@encs.concordia.ca; ymzhang@encs.concordia.ca).

limited hardware redundancy available in such a system. Some researchers sacrifice the yaw motion control to maintain the pitch and roll motion control performance when one motor encounters big fault or even failure [15]–[17]. However, in this case, it is hard to continue the assigned mission, and emergency landing should be executed. An obvious alternative is to increase physical redundancy and embed FTC within the physical redundancy structure of the system [18]. In the case of a quadrotor helicopter, it could become a hexarotor or octorotor helicopter with the increased hardware redundancy, which can also increase system performance such as increased payload capability, etc. This will significantly improve the reliability and survivability of the system due to the redundant motors [19], which can be naturally used to develop and test advanced FTC schemes. In [20], Du *et al.* analyze the controllability for a class of hexarotor helicopters subject to motor failure. When one motor fails, the hexarotor helicopter considered in [20] is uncontrollable, even though it is over-actuated compared to a quadrotor helicopter. Thus, in order to minimize flight performance degradation in the case of motor failure, an octorotor helicopter is a better choice for real applications. Motivated by this, the authors mount extra four motors under the original ones on an existing quadrotor helicopter available at the authors' lab, respectively. Compared to the octorotor helicopter used in [21] and [22], the one used in this paper is more compact, and more suitable for applications in urban and indoor environment. In fact, due to payload and better flight performance requirements for different engineering applications, more and more hexarotor and octorotor helicopters are available on the small UAVs market. Such a development and application trend also provides natural needs and platforms for developing and implementing FTC strategies on these UAVs towards satisfaction of strict safety and reliability demands by US Federal Aviation Administration (FAA) or other country's licensing & certificating authorities for practical and commercial uses of developed UAVs. With the increase of available redundant actuators, the problem of allocating them to achieve the desired forces and moments becomes non-unique and far more complex. Such redundancy has called for effective control allocation schemes to distribute the required control forces and moments over the available actuators. In particular, in the case of actuator fault/failure, an effective control re-allocation of the remaining healthy actuators is needed to achieve acceptable performance.

As one of the effective control techniques for controlling over-actuated systems, control allocation (CA) approach offers the advantage of modular design, where the design of the high-level control strategy is independent of the actuator configuration by introducing the virtual control module and control allocation module, respectively. The allocation of the virtual control signals to the individual actuators is accomplished within the control allocation module. Important issues such as input saturation, rate constraints, and actuator fault-tolerance can also be handled within this module. The CA problem without considering system fault/failure has been intensively studied following the work of Durham [23]. In the presence of actuator fault/failure, an effective re-allocation of the virtual control signals to the remaining healthy actuators is needed to maintain system performance, which is referred to as reconfigurable control allocation problem [24]. In the context of reconfigurable fault-tolerant control, Zhang *et al.* [24], [25] present the concept of control allocation and re-allocation for aircraft with redundant control effectors. Moreover, for the sake of the overall system performance and stability, a high-level virtual controller is needed to provide the desired virtual control signals for the low-level control allocation module.

Sliding mode control (SMC) is known as a robust control approach to maintain system performance and keep the closed-loop system insensitive to uncertainties and disturbances [26]. Due to this advantage of SMC over the other nonlinear control approaches, it has been extensively employed in the FTC area [27]–[33]. However, only SMC itself cannot directly deal with complete actuator failure without any redundant actuators [34]. In particular, most studies of FTC using SMC technique on multirotor helicopters only deal with partial loss of control effectiveness fault in actuators [28], [33]. Since the publication of the early works [24], [25] on combination of a baseline control law with a reconfigurable control allocation scheme for achieving fault-tolerant control, SMC and other baseline/virtual control laws combined with control allocation schemes have been developed in recent years [27], [34]–[36]. In this case, the virtual control signals will be re-allocated to the remaining healthy actuators in the presence of actuator fault/failure without reconfiguring the high-level SMC to inherit the original system performance. However, most of the reconfigurable control allocation schemes in the literature only focus on the allocation of the virtual control signals over the available actuators to minimize the designed performance function and rarely concern the stability of the overall system. If the control allocation module fails to meet the required virtual control signals, the performance of the overall system will be degraded or even the stability of the overall system cannot be maintained anymore.

In this paper, a novel control scheme by combining adaptive sliding mode control with control allocation is proposed, which can accommodate simultaneous actuator faults in the same grouped actuators and maintain the stability of the closed-loop system. Here, the grouped actuators stands for the actuators which have the same/similar control effects on the aircraft or specially on the octorotor helicopter platform developed in this work. The main contributions of this paper are summarized as follows:

1) The stability of the entire control system is considered and proven theoretically. When control allocation module fails to meet the required virtual control signals, the tracking performance and stability of the closed-loop system can still be maintained with the proposed control scheme.
2) The proposed control scheme is able to tolerate both single actuator fault and simultaneous actuator faults, where not only the control re-allocation scheme needs to be triggered to redistribute more control signals to the less affected actuators, but also the synthesized adaptive scheme will be employed to adjust the control gains for the high-level control module to compensate the virtual control error generated by the low-level control allocation

This article has been accepted for publication in a future issue of this journal, but has not been fully edited. Content may change prior to final publication. Citation information: DOI 10.1109/TIE.2017.2772153, IEEE Transactions on Industrial Electronics

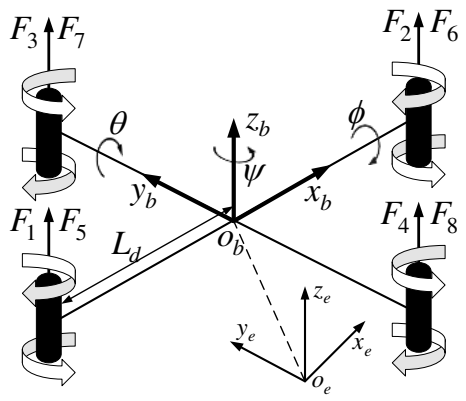

Fig. 1. Configuration of the modified octorotor helicopter.

module.

3) The design of the adaptive control law can significantly reduce the use of discontinuous control strategy of SMC, which can help to suppress control chattering. Moreover, the overestimation of control gains is avoided with the construction of adaptation law. The adaptation ceases once the sliding surface is within the defined boundary layer.

The remainder of this paper is organized as follows. The modeling of the modified octorotor helicopter is described in Section II. Then in Section III, the detailed design procedure of the proposed adaptive FTC scheme is presented. The experimental results based on the modified octorotor helicopter are followed in Section IV to demonstrate the effectiveness of the proposed control scheme. Finally, general conclusions of this paper are summarized in Section V.

II. Problem Formulation

A. Modeling of the Octorotor Helicopter

In this section, the mathematical model of the octorotor helicopter is presented, which is modified based on a quadrotor helicopter produced by Quanser. The original quadrotor helicopter is very well modeled with four rotors in a cross configuration. All the rotors' axes of rotation are fixed and parallel. The only thing that can vary is the speed of the rotor. Each pair of the opposite rotors turns the same way. In fact, in order to keep the compact structure of the modified octorotor helicopter, the extra four rotors should be added just under the original ones, respectively. The rotation direction of each added rotor is set opposite to the original one inspired by coaxial helicopter, which can counteract the yaw torque mutually as depicted in Fig. 1.

1) Kinematic Equations: In order to model the octorotor helicopter, two coordinate systems are employed: the local navigation frame and the body-fixed frame [4]. The axes of the body-fixed frame are denoted as (o_b, x_b, y_b, z_b) and the axes of the local navigation frame are denoted as (o_e, x_e, y_e, z_e). The position $X^I = [x_e, y_e, z_e]^T$ and attitude $\Theta^I = [\phi, \theta, \psi]^T$ of the octorotor helicopter are defined in the local navigation frame which is regarded as the inertial reference frame. The translational velocity $V^B = [u, v, w]^T$ and rotational velocity $\omega^B = [p, q, r]^T$ are defined in the body-fixed frame. For facilitating the modeling of the octorotor helicopter, a transformation matrix from the body-fixed frame to the inertial reference frame is given to help link the translational velocities in both reference frames [37]:

$$R_B^I = \begin{bmatrix} c\theta c\psi & s\phi s\theta c\psi - c\phi s\psi & c\phi s\theta c\psi + s\phi s\psi \\ c\theta s\psi & s\phi s\theta s\psi + c\phi c\psi & c\phi s\theta s\psi - s\phi c\psi \\ -s\theta & s\phi c\theta & c\phi c\theta \end{bmatrix} \quad (1)$$

where $s\phi = \sin(\phi)$ and $c\phi = \cos(\phi)$, which are similar for both θ and ψ.

Then, another transformation matrix is determined to resolve the Euler angle rates into rotational velocities defined in the body-fixed frame as follows:

$$T_B^I = \begin{bmatrix} 1 & s\phi t\theta & c\phi t\theta \\ 0 & c\phi & -s\phi \\ 0 & s\phi/c\theta & c\phi/c\theta \end{bmatrix} \quad (2)$$

where $t\theta = \tan(\theta)$.

According to the above transformation matrices, it is possible to describe the kinematic equations in the following matrix manner [38]:

$$\dot{\xi}^I = \begin{bmatrix} \dot{X}^I \\ \dot{\Theta}^I \end{bmatrix} = \begin{bmatrix} R_B^I & 0_{3\times3} \\ 0_{3\times3} & T_B^I \end{bmatrix} \begin{bmatrix} V^B \\ \omega^B \end{bmatrix} = J_B^I \nu^B. \quad (3)$$

2) Dynamic Equations: In order to derive the dynamic equations of the octorotor helicopter, two assumptions need to be addressed firstly [38]:

i) The origin of the body-fixed frame coincides with the center of mass (COM) of the octorotor helicopter.

ii) The axes of the body-fixed frame are coincident with the principal axes of inertia of the octorotor helicopter.

With the above assumptions, the inertial matrix becomes diagonal, and there is no need to take another point, COM, into account for deriving the dynamic equations.

By employing the Newton-Euler formulation, the forces and moments equations can be expressed as below [38]:

$$\begin{bmatrix} F^I \\ \tau^B \end{bmatrix} = \begin{bmatrix} m & 0_{3\times3} \\ 0_{3\times3} & I \end{bmatrix} \begin{bmatrix} \ddot{X}^I \\ \dot{\omega}^B \end{bmatrix} + \begin{bmatrix} 0 \\ \omega^B \times I\,\omega^B \end{bmatrix} \quad (4)$$

where $F^I = [F_x\ F_y\ F_z]^T$ and $\tau^B = [\tau_x\ \tau_y\ \tau_z]^T$ are the force and moment vectors with respect to the inertial reference frame and the body-fixed frame, respectively. m is the total mass of the octorotor helicopter, and I is the diagonal inertial matrix defined as $I = diag([I_{xx}\ I_{yy}\ I_{zz}])$.

The forces on the octorotor helicopter are composed of three parts: gravitation (G), thrust (T), and the translational motion induced drag force (D), given by $F^I = G + R_B^I T + D$. By substituting this equation into (4), it can be obtained that,

$$\begin{bmatrix} \ddot{x}_e \\ \ddot{y}_e \\ \ddot{z}_e \end{bmatrix} = \begin{bmatrix} 0 \\ 0 \\ -g \end{bmatrix} + \frac{1}{m} \begin{bmatrix} (c\phi s\theta c\psi + s\phi s\psi)U_z \\ (c\phi s\theta s\psi - s\phi c\psi)U_z \\ (c\phi c\theta)U_z \end{bmatrix} + \frac{1}{m} \begin{bmatrix} -K_1\dot{x}_e \\ -K_2\dot{y}_e \\ -K_3\dot{z}_e \end{bmatrix}. \quad (5)$$

where K_1, K_2, K_3 are the drag coefficients and g is the acceleration of gravity. Similarly, the moments are composed

of gyroscopic torque (M_g), the torque generated by the rotors (U), and the rotational motion induced torque (M_f), described as $\tau^B = M_g + M_T + M_f$. Then, by substituting this equation into (4), the following equation can be acquired:

$$\begin{bmatrix} \dot{p} \\ \dot{q} \\ \dot{r} \end{bmatrix} = I^{-1} \left(- \begin{bmatrix} 0 & I_{zz}r & -I_{yy}q \\ -I_{zz}r & 0 & I_{xx}p \\ I_{yy}q & -I_{xx}p & 0 \end{bmatrix} \begin{bmatrix} p \\ q \\ r \end{bmatrix} + I_r \begin{bmatrix} -q \\ p \\ 0 \end{bmatrix} \Omega + \begin{bmatrix} U_\phi \\ U_\theta \\ U_\psi \end{bmatrix} + \begin{bmatrix} -K_4 L_d \dot{\phi} \\ -K_5 L_d \dot{\theta} \\ -K_6 \dot{\psi} \end{bmatrix} \right) \tag{6}$$

where I_r is the inertial moment of the rotor and L_d is the distance between motor and the COM of the octorotor helicopter. K_4, K_5, K_6 are the drag coefficients and $\Omega = \Omega_1 + \Omega_2 - \Omega_3 - \Omega_4 - \Omega_5 - \Omega_6 + \Omega_7 + \Omega_8$ is the residual of the overall rotors' speed.

In order to facilitate the controller design, assume that the changes of roll and pitch angles are very small, so that the transformation matrix T_B^I as shown in (2) is very close to an identity matrix. Therefore, the rotational velocities can be replaced directly by Euler angle rates as shown below:

$$\begin{bmatrix} \ddot{\phi} \\ \ddot{\theta} \\ \ddot{\psi} \end{bmatrix} \approx I^{-1} \left(- \begin{bmatrix} 0 & I_{zz}\dot{\psi} & -I_{yy}\dot{\theta} \\ -I_{zz}\dot{\psi} & 0 & I_{xx}\dot{\phi} \\ I_{yy}\dot{\theta} & -I_{xx}\dot{\phi} & 0 \end{bmatrix} \begin{bmatrix} \dot{\phi} \\ \dot{\theta} \\ \dot{\psi} \end{bmatrix} + I_r \begin{bmatrix} -\dot{\theta} \\ \dot{\phi} \\ 0 \end{bmatrix} \Omega + \begin{bmatrix} U_\phi \\ U_\theta \\ U_\psi \end{bmatrix} + \begin{bmatrix} -K_4 L_d \dot{\phi} \\ -K_5 L_d \dot{\theta} \\ -K_6 \dot{\psi} \end{bmatrix} \right). \tag{7}$$

3) Control Mixing: Due to the configuration of the octorotor helicopter, the attitude (ϕ, θ) is coupled with the position (x_e, y_e), and a pitch or roll angle is required in order to move the octorotor helicopter along x_e or y_e direction. The virtual control inputs (U_z, U_ϕ, U_θ, U_ψ) as shown in (5) and (7) for moving and stabilizing the octorotor helicopter are mapped from the thrusts generated by the eight independent rotors. The relationship between the generated thrust T_j and the jth motor input is given as $T_j = K_u \frac{\omega}{s+\omega} u_j$, $j = 1, 2, \ldots, 8$, where K_u is a positive gain, ω is the actuator bandwidth, and u_j is pulse-width modulation (PWM) input of the jth motor. In order to make it easy to model the actuator dynamics, a new variable u_j^* is defined to represent the dynamics of the jth motor as $u_j^* = \frac{\omega}{s+\omega} u_j$. The corresponding torque τ_j generated by the jth rotor is modeled as $\tau_j = K_y u_j^*$, where K_y is a positive gain.

According to the configuration of the octorotor helicopter as shown in Fig. 1, the total thrust U_z along z direction is given by the sum of the thrusts from the eight rotors $U_z = T_1 + T_2 + T_3 + T_4 + T_5 + T_6 + T_7 + T_8$. The positive roll moment is generated by increasing the thrusts in the left rotors (T_3 and T_7) and decreasing the thrusts in the right rotors (T_4 and T_8) simultaneously $U_\phi = L_d(T_3 - T_4 + T_7 - T_8)$. Similarly, the positive pitch moment is generated by increasing the thrusts in the rear rotors (T_1 and T_5) and decreasing the thrusts in the front rotors (T_2 and T_6) simultaneously $U_\theta = L_d(T_1 - T_2 + T_5 - T_6)$, and the yaw moment is caused by the difference between the torques exerted by the four clockwise and another four counter-clockwise rotating rotors $U_\psi = (\tau_1 + \tau_2 - \tau_3 - \tau_4 - \tau_5 - \tau_6 + \tau_7 + \tau_8)$.

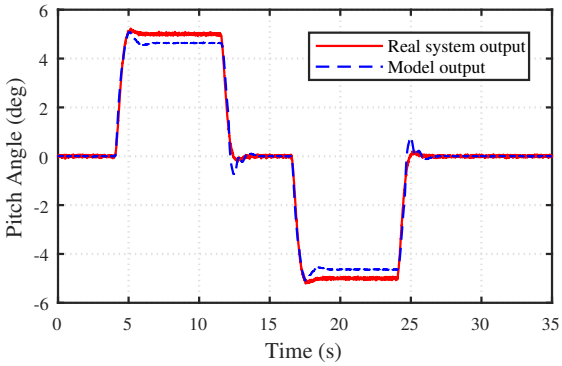

Fig. 2. The testing result of model effectiveness for one of the octorotor helicopter outputs.

In order to validate the effectiveness of the constructed mathematical model of the octorotor helicopter, a set of control inputs is introduced to both the real system and the constructed model in an open-loop fashion. As shown in Fig. 2, the constructed mathematical model can represent the real system very well.

B. Problem Statement

Consider a nonlinear affine system:

$$\dot{x}(t) = f(x(t), t) + h(x(t), t)\nu(t) + d(t) \tag{8}$$

$$\nu(t) = B_u L(t) u(t) \tag{9}$$

where (9) represents the relationship between the virtual control input and the actual control input [39]. $u(t) \in \mathbb{R}^m$ is the control input, $\nu(t) \in \mathbb{R}^n$ is the virtual control input, and $x(t) \in \mathbb{R}^n$ is the state vector. The vector $f(x(t), t) \in \mathbb{R}^n$ is a nonlinear function and $h(x(t), t) \in \mathbb{R}^{n \times n}$ is a diagonal matrix. $d(t) \in \mathbb{R}^n$ represents disturbance which is assumed to be unknown but bounded, $\|d(t)\| \leq D$. $B_u \in \mathbb{R}^{n \times m}$ is the control effectiveness matrix. $L(t) = diag([l_1(t), \cdots, l_m(t)])$ represents the control effectiveness level of the actuators, where $l_j(t)_{(j=1,\ldots,m)}$ is a scalar satisfying $0 \leq l_j(t) \leq 1$. If $l_j(t) = 1$, the jth actuator works perfectly, otherwise, the jth actuator suffers certain level of fault with a special case $l_j(t) = 0$ denoting the complete failure of the jth actuator [34].

In this paper, control allocation problem refers to the distribution of the virtual control signals over the available actuators. In a faulty condition where $l_j(t) < 1$, given the desired virtual control signal $\nu_d(t)$, the solution $u(t)$ is searched such that $\nu_d(t) = B_u L(t) u(t)$ is satisfied. To facilitate the controller development, the following assumptions with respect to the nonlinear affine system (8)–(9) are made.

Assumption 1: Matrix B_u has the full row rank, i.e., $rank(B_u) = n < m$.

Assumption 2: The control input $u(t)$ lies in a compact set Ω_u described as:

$$u(t) \in \Omega_u = \{u(t) \in \mathbb{R}^m | u_{\min} \leq u(t) \leq u_{\max}\} \tag{10}$$

This article has been accepted for publication in a future issue of this journal, but has not been fully edited. Content may change prior to final publication. Citation information: DOI 10.1109/TIE.2017.2772153, IEEE Transactions on Industrial Electronics

where $u_{\min} = \{u_{1\min}, u_{2\min}, \cdots, u_{m\min}\}$ and $u_{\max} = \{u_{1\max}, u_{2\max}, \cdots, u_{m\max}\}$.

Assumption 1 implies a necessary condition for a system to be over-actuated. In this paper, the number of redundant actuators is chosen to be four in order to accommodate actuator failures and also due to the special symmetrical configuration of the original quadrotor helicopter. In this case, the rank of the control distribution matrix B_u is four. The control input constraints described in Assumption 2 are the same for all the actuators in this paper. For simplicity of the expression, the notation t is omitted in the following sections, e.g., $x(t)$ is expressed as x.

C. Formulation of the Transformed System

The actuators used in the octorotor helicopter can provide not only required moments but also forces to maintain the demanded attitude and height. Therefore, the attitude and height controllers are both directly related to the actuators. Then, the state vector is defined as follows:

$$\begin{aligned} x &= [z_e \;\; \dot{z}_e \;\; \phi \;\; \dot{\phi} \;\; \theta \;\; \dot{\theta} \;\; \psi \;\; \dot{\psi}]^T \\ &= [x_1 \;\; x_2 \;\; x_3 \;\; x_4 \;\; x_5 \;\; x_6 \;\; x_7 \;\; x_8]^T. \end{aligned} \tag{11}$$

With this state vector, the dynamic equations of the octorotor helicopter in (5) and (7) can be resolved into the following subsystems. Height subsystem: $\dot{x}_1 = x_2$, $\dot{x}_2 = f_1(x) + h_1\nu_1 + d_1$ with $f_1(x) = -g$, $h_1 = \cos\phi\cos\theta/m$, and $d_1 = -K_3\dot{z}_e/m$; Roll subsystem: $\dot{x}_3 = x_4$, $\dot{x}_4 = f_2(x) + h_2\nu_2 + d_2$ with $f_2(x) = x_6x_8(I_{yy} - I_{zz})/I_{xx}$, $h_2 = 1/I_{xx}$, and $d_2 = -I_r\dot{\theta}\Omega/I_{xx} - K_4L_d\dot{\phi}/I_{xx}$; Pitch subsystem: $\dot{x}_5 = x_6$, $\dot{x}_6 = f_3(x) + h_3\nu_3 + d_3$ with $f_3(x) = x_4x_8(I_{zz} - I_{xx})/I_{yy}$, $h_3 = 1/I_{yy}$, and $d_3 = I_r\dot{\phi}\Omega/I_{yy} - K_5L_d\dot{\theta}/I_{yy}$; Yaw subsystem: $\dot{x}_7 = x_8$, $\dot{x}_8 = f_4(x) + h_4\nu_4 + d_4$ with $f_4(x) = x_4x_6(I_{xx} - I_{yy})/I_{zz}$, $h_4 = 1/I_{zz}$, and $d_4 = -K_6\dot{\psi}/I_{zz}$. Therefore, in this transformed system, there are four system outputs, four actuators and four redundant actuators. Then, each subsystem can be written as a single-input nonlinear system with the help of the virtual control input given by:

$$\begin{aligned} \dot{x}_{2i-1} &= x_{2i} \\ \dot{x}_{2i} &= f_i(x) + h_i\nu_i + d_i \end{aligned} \tag{12}$$

where $i = 1, 2, 3, 4$ represents each subsystem.

III. Adaptive Fault-Tolerant Control Strategy

In this section, an adaptive sliding mode control allocation (ASMCA) scheme is designed to accommodate actuator faults for the modified octorotor helicopter. The control allocation and re-allocation scheme itself could compensate actuator fault/failure without affecting the high-level control performance when only one of the actuators in the same group malfunctions. In the case of simultaneous actuator faults in the same group, not only the control re-allocation scheme should be triggered to redistribute more control signals to the less affected actuators, but also the synthesized adaptive scheme is employed to adjust the control gains for the high-level sliding mode controller to compensate the virtual control error. In such a way, the overall system performance can be maintained in both single and simultaneous actuator fault/failure conditions.

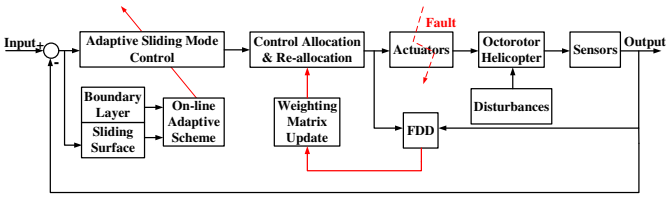

Fig. 3. The schematic of the proposed adaptive control strategy.

The schematic of the proposed control strategy is depicted in Fig. 3.

A. Design of Sliding Mode Control

The design of a sliding mode controller is typically composed of two steps. The first step features the construction of a sliding surface, on which the system performance could be maintained as expected. The second step is concerned with the selection of the control law to force the sliding variable reach the sliding surface, and hereafter keep the sliding motion within the close neighborhood of the sliding surface. However, during the reaching phase, the insensitivity of the controller cannot be ensured. One way to solve this problem is to employ integral sliding mode control scheme, such that the robustness of the system can be guaranteed throughout the entire response of the system starting from the initial time instance [40].

The integral sliding surface for the system is defined by the following set:

$$S_i = \{x \in \mathbb{R}^n : \; \sigma_i(x) = 0\}. \tag{13}$$

The switching function $\sigma_i(x)$ is defined as:

$$\sigma_i(x) = \sigma_{i0}(x) + z_i \tag{14}$$

$$\sigma_{i0}(x) = C_i^T x \tag{15}$$

where $C_i \in \mathbb{R}^n$, $\sigma_{i0}(x)$ is the linear combination of the states, which is similar to the conventional sliding mode design, and z_i includes the integral term which will be determined below.

First of all, assume that there are no actuator faults and disturbances, i.e., $d_i = 0$ and $L = I^{m\times m}$, hence the ideal system can be given by the following equations:

$$\dot{x}_{2i}^0 = f_i^0(x^0) + h_i^0\nu_i^0 \tag{16}$$

$$\nu_i^0 = B_{ui}^0 u_0 \tag{17}$$

$$x(t_0) = x^0(t_0) \tag{18}$$

where x_{2i}^0 denotes the state trajectory of the ideal system under the control of u_0.

The choice of z_i is determined by the following equations in order to guarantee that $\sigma_i(x, t_0) = 0$.

$$\dot{z}_i = -C_i^T(f_i^0(x^0) + h_i^0\nu_i^0) \tag{19}$$

$$z_i(0) = -C_i^T x(t_0) \tag{20}$$

i.e.,

$$z_i = -C_i^T[x(t_0) + \int_{t_0}^{t}(f_i^0(x^0(\tau)) + h_i^0\nu_i^0(\tau))d\tau] \tag{21}$$

The term $x(t_0) + \int_{t_0}^{t}(f_i^0(x^0(\tau)) + h_i^0\nu_i^0(\tau))d\tau$ in (21) can be regarded as the trajectory of the ideal system under the nominal virtual control ν_i^0. That is to say, the motion equation of the sliding variable coincides with that of the ideal system without faults and disturbances. Due to this definition of z_i, $\sigma_i(x(t_0), t_0) = \sigma_{i0}(x(t_0), t_0) + z_i(0) = 0$ can be obtained and sliding motion occurs at the initial time instance t_0. Hence, the system trajectory under integral SMC starts from the designed sliding surface and the reaching phase is eliminated accordingly in contrast with conventional SMC.

Then, after obtaining the sliding surface, the problem is to design an appropriate control law to make the sliding surface attractive. The design problem can be formulated as that, given $x(t_0) = x^0(t_0)$, the identity $x = x^0$ should be guaranteed all the time $t \geq t_0$. According to this requirement, the control law is designed in the following form:

$$\nu_i = \nu_{i0} + \nu_{i1} \tag{22}$$

where ν_{i0} is the continuous nominal control part to stabilize the ideal system in (16) and guide it to a given trajectory with satisfactory accuracy. ν_{i1} is the discontinuous control part for compensating the perturbations and disturbances in order to ensure the sliding motion.

For $\forall i = 1, 2, 3, 4$, denoting x_{2i-1}^d and x_{2i}^d as the desired trajectories, the tracking errors can be defined as $\tilde{x}_{i1} = x_{2i-1} - x_{2i-1}^d$ and $\tilde{x}_{i2} = x_{2i} - x_{2i}^d$. According to the definition of the integral sliding surface in (14), the switching function can be rewritten as:

$$\sigma_{i0} = c_i\tilde{x}_{i1} + \tilde{x}_{i2} \tag{23}$$

$$\begin{aligned} \dot{z}_i &= -c_i\tilde{x}_{i2} + k_{i2}\tilde{x}_{i2} + k_{i1}\tilde{x}_{i1} \\ z_i(0) &= -c_i\tilde{x}_{i1}(t_0) - \tilde{x}_{i2}(t_0) \end{aligned} \tag{24}$$

Such that,

$$\sigma_i = \tilde{x}_{i2} + k_{i2}\tilde{x}_{i1} + k_{i1}\int_{t_0}^{t}\tilde{x}_{i1}(\tau)d\tau - k_{i2}\tilde{x}_{i1}(t_0) - \tilde{x}_{i2}(t_0). \tag{25}$$

From the switching function defined in (25), it can be observed that regardless of the values of x_{2i-1}^d and x_{2i}^d at t_0, the sliding variable is already on the sliding surface once the sliding motion begins. The positive constant c_i is used to define the switching function as shown in (23) and (24). However, c_i does not appear in (25) which means c_i is not necessary here to obtain the sliding surface. Therefore, no matter what the value of c_i is, the sliding motion will not be affected.

In order to analyze the sliding motion associated with the switching function as shown in (25), the time derivative of the switching function is computed as follows:

$$\dot{\sigma}_i = \dot{\tilde{x}}_{i2} + k_{i2}\tilde{x}_{i2} + k_{i1}\tilde{x}_{i1}. \tag{26}$$

The equivalent control ν_{i0} is designed by equalizing $\dot{\sigma}_i = 0$. In this case, the disturbance d_i is omitted, and the system is given as:

$$\dot{x}_{2i} = f_i(x) + h_i\nu_i. \tag{27}$$

Substituting (27) into (26) yields

$$f_i(x) + h_i\nu_i - \dot{x}_{2i}^d + k_{i2}\tilde{x}_{i2} + k_{i1}\tilde{x}_{i1} = 0. \tag{28}$$

In the presence of disturbance d_i, substituting (28) into (12), the resultant error dynamics can be written as:

$$\dot{\tilde{x}}_{i2} + k_{i2}\tilde{x}_{i2} + k_{i1}\tilde{x}_{i1} = d_i. \tag{29}$$

One can easily tell from (29) that no matter what values of the constant parameters k_{i1} and k_{i2} are, the tracking error $\tilde{x}_{i1}$ and its derivatives $\tilde{x}_{i2}$ and $\dot{\tilde{x}}_{i2}$ will not tend to zero due to the presence of disturbance. To this end, a discontinuous control part is synthesized to reject the disturbance as shown below:

$$\nu_{i1} = -h_i^{-1}k_{ci}\text{sign}(\sigma_i) \tag{30}$$

where k_{ci} is a positive high gain which rejects the disturbance and makes the sliding surface attractive.

Therefore, the control law can be developed as:

$$\nu_i = h_i^{-1}(\dot{x}_{2i}^d - k_{i2}\tilde{x}_{i2} - k_{i1}\tilde{x}_{i1} - f_i(x)) - h_i^{-1}k_{ci}sign(\sigma_i). \tag{31}$$

However, in order to account for disturbances, the control discontinuity is increased which may lead to control chattering. One can remove this condition by smoothing the control discontinuity in a thin boundary layer neighboring the sliding surface. The boundary layer is formulated as follows [41]:

$$\bar{B} = \{\tilde{x}_{i1}, \tilde{x}_{i2}, |\sigma_i| \leq \Phi_i\} \tag{32}$$

where Φ_i is the boundary layer thickness with positive value.

Accordingly, the feedback control law becomes:

$$\nu_i = h_i^{-1}(\dot{x}_{2i}^d - k_{i2}\tilde{x}_{i2} - k_{i1}\tilde{x}_{i1} - f_i(x)) - h_i^{-1}k_{ci}sat(\sigma_i/\Phi_i) \tag{33}$$

where the sat function is defined as:

$$sat(\sigma_i/\Phi_i) = \begin{cases} sign(\sigma_i) & if \quad |\sigma_i| \geq \Phi_i \\ \sigma_i/\Phi_i & if \quad |\sigma_i| < \Phi_i \end{cases}. \tag{34}$$

B. Adaptive Fault-Tolerant Control Allocation

One way to achieve fault-tolerance for control allocation scheme is to solve a constrained optimization problem on-line at every sampling instant. The 2-norm (quadratic) formulation seems to be favorable over the 1-norm (linear) formulation since the solution tends to combine the use of all control surfaces rather than just a few [42].

Considering the implementation of the control scheme in real system, the control re-allocation needs to be triggered instantly when actuator fault/failure occurs. Given the system in (8), the control input u is computed employing quadratic optimization approach, such that conditions as shown in (9) and (10) can be satisfied.

Lemma 1: The quadratic programming (QP) approach based on minimizing control input can be described as [27]:

$$\begin{aligned} J &= arg\min_{u} u^TWu \\ s.t. \quad &\nu_i = B_{ui}u \end{aligned} \tag{35}$$

and it has an explicit solution as follows [27]:

$$u = WB_{ui}^T(B_{ui}WB_{ui}^T)^{-1}\nu_i \tag{36}$$

where $W = W^T = diag([w_1, w_2, \ldots, w_m])$ is a symmetric positive definite weighting matrix, $B_{ui} \in \mathbb{R}^{n\times m}$ is the control

effectiveness matrix directly related to actuators, and ν_i is the virtual control signal from the high-level controller.

Since the considered system is over-actuated and in principle there exists a set of admissible control inputs u. When some of the actuators encounter faults/failures, the control allocation scheme should have the capability to redistribute the control efforts from the faulty actuators to the healthier ones. In order to achieve this goal, the commonly used approach is to change the weighting matrix W which requires fault information from the fault detection and diagnosis module. The larger of the corresponding gain in the weighting matrix, the less of the control input to the corresponding actuator.

In the case of single actuator fault/failure, the weighting matrix is updated according to the fault information from the fault detection and diagnosis module without affecting the high-level controller, namely, $w_{j(j=1,2,\ldots,m)} = 1/l_j$. In this situation, more control efforts will be distributed to the healthier actuators. Specially, when the jth actuator experiences complete failure, the corresponding weighting parameter w_j will become infinity which means there will be no control effort distributed to this actuator.

In the case of simultaneous actuator faults, where control allocation and re-allocation scheme fails to maintain the overall system stability, an adaptive scheme is synthesized to compensate this faulty condition. In this circumstance, conditions described in (9) and (10) could not be satisfied at the same time due to the error between the generated virtual control signal from the control allocation module and the desired one from the high-level sliding mode control module.

Let $\nu_i = \nu_{id} + \tilde{\nu}_i$, the following system dynamics can be obtained:

$$\dot{x}_{2i} = f_i(x) + h_i\nu_{id} + h_i\tilde{\nu}_i + d_i \tag{37}$$

where $\tilde{\nu}_i$ denotes the virtual control error.

In order to maintain the closed-loop system performance, the high-level sliding mode controller needs to be reconfigured. For this reason, an adaptive approach is employed. Observed from (37), in order to maintain the tracking performance of the high-level controller when there is error between ν_i and ν_{id}, the parameter h_i should be adjusted accordingly to eliminate this error. In this case, the term $h_i\tilde{\nu}_i$ in (37) can be expressed as $\tilde{h}_i\nu_{id}$. Therefore, (37) can be rewritten as:

$$\begin{aligned}\dot{x}_{2i} &= f_i(x) + (h_i + \tilde{h}_i)\nu_{id} + d_i \\ &= f_i(x) + \hat{h}_i\nu_{id} + d_i.\end{aligned} \tag{38}$$

In this case, denoting $\hat{\Upsilon}_i = \hat{h}_i^{-1}$ and considering the sliding surface in (25), the high-level sliding mode control law is redesigned using the estimated $\hat{\Upsilon}_i$ as follows:

$$\nu_i = \hat{\Upsilon}_i(\dot{x}_{2i}^d - k_{i2}\tilde{x}_{i2} - k_{i1}\tilde{x}_{i1} - f_i(x)) - \hat{\Upsilon}_i k_{ci} sat(\sigma_i/\Phi_i). \tag{39}$$

In order to develop the adaptive scheme to update the estimated parameter $\hat{\Upsilon}_i$, a new variable is defined based on the switching function and boundary layer as follows:

$$\sigma_{\Delta i} = \sigma_i - \Phi_i sat(\sigma_i/\Phi_i) \tag{40}$$

where $\sigma_{\Delta i}$ is the measurement of the algebraic distance between the current state and the boundary layer. It features $\dot{\sigma}_{\Delta i} = \dot{\sigma}_i$ outside the boundary layer and $\sigma_{\Delta i} = 0$ inside the boundary layer.

Based on this newly-defined variable, the on-line adaptive scheme is formulated as:

$$\dot{\hat{\Upsilon}}_i = (-\dot{x}_{2i}^d + k_{i2}\tilde{x}_{i2} + k_{i1}\tilde{x}_{i1} + f_i(x) + k_{ci} sat(\sigma_i/\Phi_i))\sigma_{\Delta i}. \tag{41}$$

With the help of the adaptive scheme, as long as the sliding variable is out of the boundary layer where the control performance is unacceptable, the adaptation will be triggered to bring the sliding variable back inside the boundary layer to maintain system tracking performance.

Remark 1: The variable $\sigma_{\Delta i}$ used to construct the adaptive scheme can cease the behavior of adaptation when the sliding variable reaches the boundary layer. Overestimation of the parameter is avoided in such a way compared to the adaptive approaches in the literature where the adaptation cannot stop due to the use of sliding variable for designing the adaptive scheme.

Theorem 1: Consider a nonlinear system with simultaneous actuator faults in the same group (both of the actuators cannot encounter complete failure together) and bounded disturbance in (12). Given the sliding surface in (25) and control input constraints in (10), by employing the feedback control laws in (36) and (39) and the on-line adaptive scheme in (41), the sliding motion will be achieved and maintained on the sliding surface to ensure the overall system tracking performance with the discontinuous gain chosen as $k_{ci} \geq \eta_i + D_i$ regardless of the virtual control error, i.e., $\tilde{\nu}_i = \nu_i - \nu_{id} \neq 0$.

Proof: Consider the following Lyapunov candidate function:

$$V_i = \frac{1}{2}[\sigma_{\Delta i}^2 + \Upsilon_i^{-1}(\hat{\Upsilon}_i - \Upsilon_i)^2]. \tag{42}$$

Then, the derivative of the selected Lyapunov candidate function would be:

$$\begin{aligned}\dot{V}_i =& \sigma_{\Delta i}\dot{\sigma}_{\Delta i} + \Upsilon_i^{-1}(\hat{\Upsilon}_i - \Upsilon_i)\dot{\hat{\Upsilon}}_i \\ =& \sigma_{\Delta i}(f_i(x) + \Upsilon_i^{-1}\hat{\Upsilon}_i(\dot{x}_{2i}^d - k_{i2}\tilde{x}_{i2} - k_{i1}\tilde{x}_{i1} - f_i(x) \\ & - k_{ci} sat(\sigma_i/\Phi_i)) + d_i - \dot{x}_{2i}^d + k_{i2}\tilde{x}_{i2} + k_{i1}\tilde{x}_{i1}) \\ & + \Upsilon_i^{-1}(\hat{\Upsilon}_i - \Upsilon_i)\dot{\hat{\Upsilon}}_i \\ =& (\Upsilon_i^{-1}\hat{\Upsilon}_i - 1)(\dot{x}_{2i}^d - k_{i2}\tilde{x}_{i2} - k_{i1}\tilde{x}_{i1} - f_i(x))\sigma_{\Delta i} \\ & + (\Upsilon_i^{-1}\hat{\Upsilon}_i - 1)\dot{\hat{\Upsilon}}_i - \Upsilon_i^{-1}\hat{\Upsilon}_i k_{ci} sat(\sigma_i/\Phi_i)\sigma_{\Delta i} + d_i\sigma_{\Delta i} \\ =& (\Upsilon_i^{-1}\hat{\Upsilon}_i - 1)(\dot{x}_{2i}^d - k_{i2}\tilde{x}_{i2} - k_{i1}\tilde{x}_{i1} - f_i(x))\sigma_{\Delta i} \\ & + (\Upsilon_i^{-1}\hat{\Upsilon}_i - 1)\dot{\hat{\Upsilon}}_i - (\Upsilon_i^{-1}\hat{\Upsilon}_i - 1)k_{ci} sat(\sigma_i/\Phi_i)\sigma_{\Delta i} \\ & - k_{ci} sat(\sigma_i/\Phi_i)\sigma_{\Delta i} + d_i\sigma_{\Delta i} \\ =& (\Upsilon_i^{-1}\hat{\Upsilon}_i - 1)[\dot{\hat{\Upsilon}}_i + (\dot{x}_{2i}^d - k_{i2}\tilde{x}_{i2} - k_{i1}\tilde{x}_{i1} - f_i(x) \\ & - k_{ci} sat(\sigma_i/\Phi_i))\sigma_{\Delta i}] - k_{ci} sat(\sigma_i/\Phi_i)\sigma_{\Delta i} + d_i\sigma_{\Delta i}.\end{aligned} \tag{43}$$

Substituting (41) into (43) leads to:

$$\begin{aligned}\dot{V}_i =& -k_{ci} sat(\sigma_i/\Phi_i)\sigma_{\Delta i} + d_i\sigma_{\Delta i} \\ \leq& -(\eta_i + D_i) sat(\sigma_i/\Phi_i)\sigma_{\Delta i} + D_i\sigma_{\Delta i} \\ \leq& -\eta_i|\sigma_{\Delta i}|.\end{aligned} \tag{44}$$

Therefore, with the proposed control scheme, the performance of the overall system is maintained in the presence of simultaneous actuator faults. □

This article has been accepted for publication in a future issue of this journal, but has not been fully edited. Content may change prior to final publication. Citation information: DOI 10.1109/TIE.2017.2772153, IEEE Transactions on Industrial Electronics

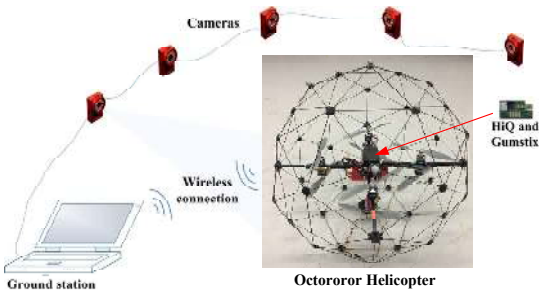

Fig. 4. The schematic of the experiment setup.

Remark 2: It can be observed that although the simultaneous actuator faults is considered during the design of the controller, the value of the discontinuous gain is not increased with the help of the adaptive scheme. This feature will preserve the original tracking performance and prevent the chattering effect in the fault-free condition.

IV. Experimental Results

In order to validate the effectiveness of the proposed adaptive fault-tolerant control strategy in real applications, some experiments are carried out in this section. The performance comparisons with normal sliding mode control allocation (NSMCA) [32] and linear quadratic regulator control allocation (LQRCA) [37] schemes are also demonstrated. The control parameters are chosen as $k_{11} = 25, k_{21} = 100, k_{31} = 100, k_{41} = 25$, $k_{12} = 10, k_{22} = 20, k_{32} = 20, k_{42} = 10$, $k_{c1} = 5, k_{c2} = 10, k_{c3} = 10, k_{c4} = 5$, and $\Phi = 0.2$. As described in [43], the robustness and reliability characteristics of the proposed approach are very important. Therefore, two experimental scenarios are demonstrated in this section to validate the effectiveness and robustness of the proposed control scheme. In scenario 1, a 100% loss of control effectiveness fault is only introduced to actuator #1 at 20 s. In scenario 2, faults are injected into two actuators at 20 s. Actuator #1 experiences a complete failure, and actuator #5 experiences 40% loss of control effectiveness fault.

A. Description of the Experimental Setup

The schematic of the experiment setup is demonstrated in Fig. 4. In the whole system, besides the octorotor helicopter itself, there is another subsystem called OptiTrack which includes twenty-four cameras as an indoor positioning system providing the position and attitude of the octorotor helicopter. For calculating the attitude of the octorotor helicopter, the on-board IMU can also be used which is called HiQ. The sampling rates for the on-board accelerometer, gyroscope and magnetometer are set as 200Hz. The control algorithm is written with Simulink blocks which can be compiled to C-code with the help of a real-time control software, namely QuaRC. The compiled code runs on an embedded Linux-based system Gumstix which uses an ARM Cortex-M4 micro-controller in real-time. Desired inputs are given from the host computer to the on-board processor of the octorotor helicopter through Wi-Fi wireless communication.

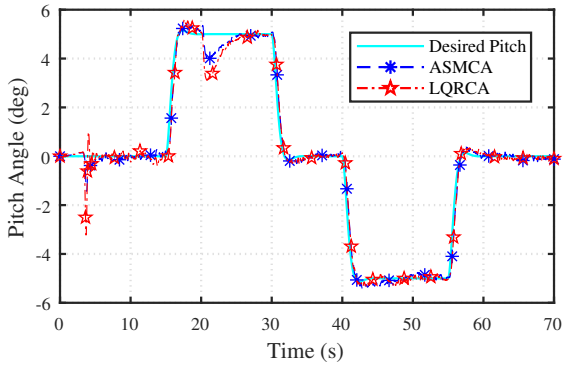

Fig. 5. Tracking performance of pitch motion in the presence of single actuator failure in real flight test.

B. Real Flight Test Results

Scenario 1: The tracking performance of pitch motion in the presence of single actuator failure is shown in Fig. 5. In this situation, the sliding variable is within the defined boundary layer as shown in Fig. 6. Therefore, the adaptive scheme will not be triggered and the tracking performance of ASMCA and NSMCA will be the same. Due to the robustness of the proposed control scheme, it has a better tracking performance than LQRCA.

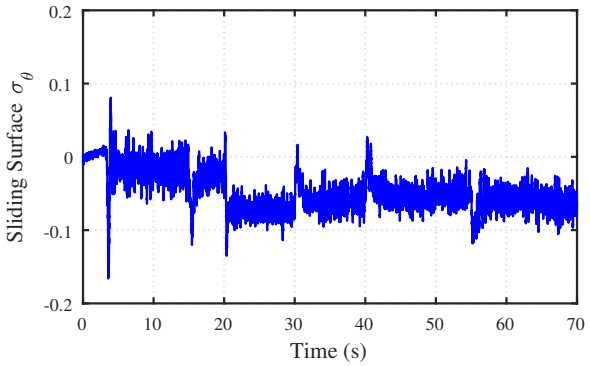

Fig. 6. Sliding surface of ASMCA for pitch motion in the presence of single actuator failure in real flight test.

Scenario 2: The tracking performance of pitch motion in the presence of simultaneous actuator faults is shown in Fig. 7. The LQRCA has the worst tracking performance after faults occur, whereas the NSMCA can gradually decrease the tracking error but still cannot achieve the original tracking performance. Compared to NSMCA and LQRCA, the proposed ASMCA can make a quicker compensation to maintain the original tracking performance with the help of the synthesized adaptive scheme. After faults occurrence, the control re-allocation scheme will be triggered firstly. Since actuator #1 completely fails, no control effort would be distributed to it, and more control effort would be distributed to the less affected actuator #5, which can be observed from Fig. 8. Note that, the range of actuator input is $[0.05\ 0.1]$. Moreover, as can be observed from Fig. 9, after faults occurrence at 20 s, due to the virtual control error caused by the simultaneous actuator

This article has been accepted for publication in a future issue of this journal, but has not been fully edited. Content may change prior to final publication. Citation information: DOI 10.1109/TIE.2017.2772153, IEEE Transactions on Industrial Electronics

faults and the corresponding inputs decrease in actuators #2 and #6 as shown in Fig. 8, there is a big deviation of the sliding surface which will trigger the high-level adaptive scheme to increase the corresponding adaptive gain which is shown in Fig. 10. With the change of the control gain of the high-level sliding mode controller, the sliding surface is brought into the boundary layer again to maintain the original tracking performance. Therefore, the proposed control scheme is a robust and reliable control strategy which represents the ability to deal with both single and simultaneous actuator faults.

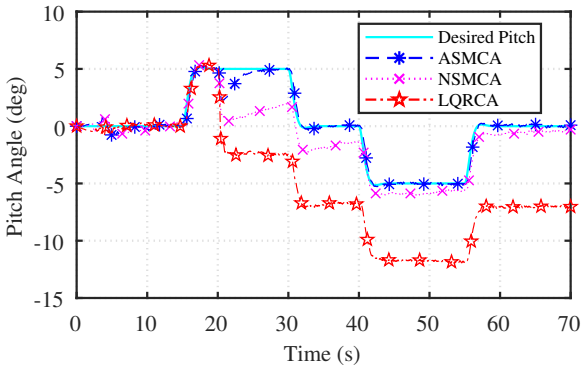

Fig. 7. Tracking performance of pitch motion in the presence of simultaneous actuator faults in real flight test.

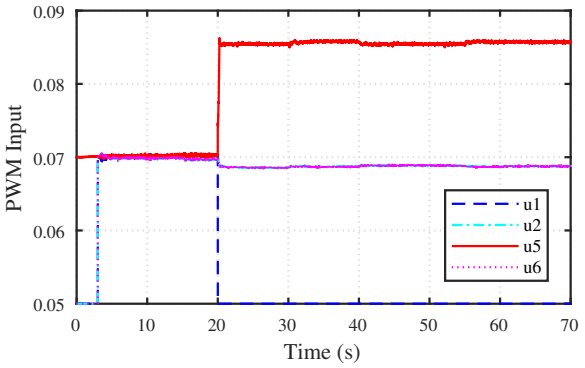

Fig. 8. Control inputs of motors in the presence of simultaneous actuator faults in real flight test.

V. Conclusions

In this paper, a novel adaptive sliding mode based control allocation scheme is proposed for a modified octorotor helicopter to accommodate simultaneous actuator faults. The control scheme includes two separate control modules: the low-level module and the high-level one. The low-level control allocation/re-allocation module is used to distribute the control signals among the required actuators, which can also reconfigure the distribution of the control signals in the presence of actuator faults. The high-level module is constructed by an adaptive sliding mode controller, which is employed to maintain the overall system tracking performance. In the case of mild faulty conditions, the control allocation/re-allocation module can successfully deal with the fault independently.

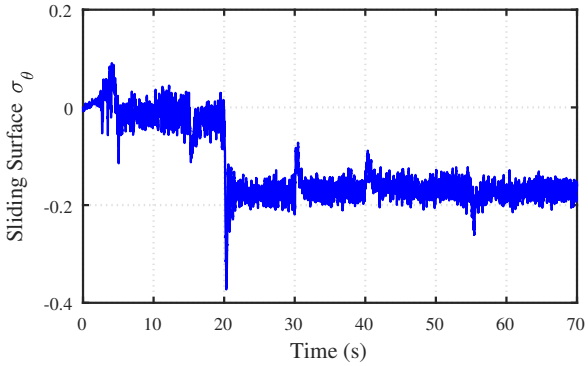

Fig. 9. Sliding surface of ASMCA for pitch motion in the presence of simultaneous actuator faults in real flight test.

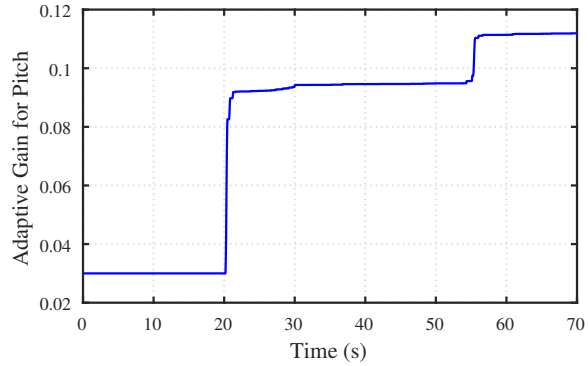

Fig. 10. Adaptive parameter of ASMCA for pitch motion in the presence of simultaneous actuator faults in real flight test.

Whereas in the case of severe faulty conditions, the adaptive scheme will be triggered to compensate the virtual control error generated by the low-level control allocation/re-allocation module. With the help of the synthesized adaptive scheme, the high-level control gains can be changed adaptively to maintain the overall system tracking performance. The demonstrated experimental results show the effectiveness and reliability of the proposed adaptive fault-tolerant control strategy in the presence of both single and simultaneous actuator faults. However, in this paper, the fault diagnosis error and delay are not considered, which is one of our future works.

References

[1] S. Yin, B. Xiao, S. X. Ding, and D. Zhou, "A review on recent development of spacecraft attitude fault tolerant control system," *IEEE Trans. Ind. Electron.*, vol. 63, no. 5, pp. 3311–3320, May. 2016.

[2] X. Yu and J. Jiang, "A survey of fault-tolerant controllers based on safety-related issues," *Annu. Rev. Control*, vol. 39, no. 1, pp. 46–57, Apr. 2015.

[3] Y. M. Zhang and J. Jiang, "Bibliographical review on reconfigurable fault-tolerant control systems," *Annu. Rev. Control*, vol. 32, no. 2, pp. 229–252, Dec. 2008.

[4] Y. M. Zhang, A. Chamseddine, C. A. Rabbath, B. W. Gordon, C. Y. Su, S. Rakheja, C. Fulford, J. Apkarian, and P. Gosselin, "Development of advanced FDD and FTC techniques with application to an unmanned quadrotor helicopter testbed," *J. Franklin I.*, vol. 350, no. 9, pp. 2396–2422, Nov. 2013.

[5] B. Xiao, M. Huo, X. Yang, and Y. M. Zhang, "Fault-tolerant attitude stabilization for satellites without rate sensor," *IEEE Trans. Ind. Electron.*, vol. 62, no. 11, pp. 7191–7202, Nov. 2015.

[6] H. Badihi, Y. M. Zhang, and H. Hong, "Wind turbine fault diagnosis and fault-tolerant torque load control against actuator faults," *IEEE Trans. Control Syst. Technol.*, vol. 23, no. 4, pp. 1351–1372, Jul. 2015.

[7] X. Liu, Z. Gao, and M. Z. Chen, "Takagi–Sugeno fuzzy model based fault estimation and signal compensation with application to wind turbines," *IEEE Trans. Ind. Electron.*, vol. 64, no. 7, pp. 5678–5689, Jul. 2017.

[8] H. Liu, D. Li, Z. Zuo, and Y. Zhong, "Robust three-loop trajectory tracking control for quadrotors with multiple uncertainties," *IEEE Trans. Ind. Electron.*, vol. 63, no. 4, pp. 2263–2274, Apr. 2016.

[9] B. Xiao and S. Yin, "A new disturbance attenuation control scheme for quadrotor unmanned aerial vehicles," *IEEE Trans. Ind. Informat.*, 2017.

[10] D. Mellinger, M. Shomin, N. Michael, and V. Kumar, "Cooperative grasping and transport using multiple quadrotors," in *Distributed Autonomous Robotic Systems*, vol. 83, pp. 545–558. Springer, 2013.

[11] M. Saska, V. Vonásek, J. Chudoba, J. Thomas, G. Loianno, and V. Kumar, "Swarm distribution and deployment for cooperative surveillance by micro-aerial vehicles," *J. Intell. Robot. Syst.*, vol. 84, no. 1, pp. 469–492, Dec. 2016.

[12] Z. Gao, X. Liu, and M. Z. Chen, "Unknown input observer-based robust fault estimation for systems corrupted by partially decoupled disturbances," *IEEE Trans. Ind. Electron.*, vol. 63, no. 4, pp. 2537–2547, Apr. 2016.

[13] M. H. Amoozgar, A. Chamseddine, and Y. M. Zhang, "Experimental test of a two-stage Kalman filter for actuator fault detection and diagnosis of an unmanned quadrotor helicopter," *J. Intell. Robot. Syst.*, vol. 70, no. 1-4, pp. 107–117, Apr. 2013.

[14] F. Chen, Q. Wu, B. Jiang, and G. Tao, "A reconfiguration scheme for quadrotor helicopter via simple adaptive control and quantum logic," *IEEE Trans. Ind. Electron.*, vol. 62, no. 7, pp. 4328–4335, Jul. 2015.

[15] M. W. Mueller and R. D'Andrea, "Stability and control of a quadrocopter despite the complete loss of one, two, or three propellers," in *Proc. IEEE Int. Conf. on Robot. & Autom.*, pp. 45–52, May–Jun. 2014.

[16] A. Lanzon, A. Freddi, and S. Longhi, "Flight control of a quadrotor vehicle subsequent to a rotor failure," *J. Guid. Control Dynam.*, vol. 37, no. 2, pp. 580–591, Mar.–Apr. 2014.

[17] P. Lu and E.-J. Van Kampen, "Active fault-tolerant control for quadrotors subjected to a complete rotor failure," in *Proc. IEEE Int. Conf. on Intell. Robot. and Syst.*, pp. 4698–4703, Dec. 2015.

[18] S. Osder, "Practical view of redundancy management application and theory," *J. Guid. Control Dynam.*, vol. 22, no. 1, pp. 12–21, Jan. 1999.

[19] A. Chamseddine, D. Theilliol, I. Sadeghzadeh, Y. M. Zhang, and P. Weber, "Optimal reliability design for over-actuated systems based on the MIT rule: Application to an octocopter helicopter testbed," *Reliab. Eng. Syst. Safe.*, vol. 132, pp. 196–206, Dec. 2014.

[20] G.-X. Du, Q. Quan, and K.-Y. Cai, "Controllability analysis and degraded control for a class of hexacopters subject to rotor failures," *J. Intell. Robot. Syst.*, vol. 78, no. 1, pp. 143–157, Apr. 2015.

[21] V. G. Adîr and A. M. Stoica, "Integral LQR control of a star-shaped octorotor," *Incas Bulletin*, vol. 4, no. 2, pp. 1–16, 2012.

[22] B. Arain and F. Kendoul, "Real-time wind speed estimation and compensation for improved flight," *IEEE Trans. Aerosp. Electron. Syst.*, vol. 50, no. 2, pp. 1599–1606, Apr. 2014.

[23] W. C. Durham, "Constrained control allocation," *J. Guid. Control Dynam.*, vol. 16, no. 4, pp. 717–725, Jul.–Aug. 1993.

[24] Y. M. Zhang, V. S. Suresh, B. Jiang, and D. Theilliol, "Reconfigurable control allocation against aircraft control effector failures," in *Proc. IEEE Int. Conf. on Control Appl.*, pp. 1197–1202, Oct. 2007.

[25] Y. M. Zhang, C. A. Rabbath, and C. Y. Su, "Reconfigurable control allocation applied to an aircraft benchmark model," in *Proc. Am. Control Conf.*, pp. 1052–1057, Jun. 2008.

[26] V. Utkin, "Variable structure systems with sliding modes," *IEEE Trans. Autom. Control*, vol. 22, no. 2, pp. 212–222, Apr. 1977.

[27] H. Alwi and C. Edwards, "Fault tolerant control using sliding modes with on-line control allocation," *Automatica*, vol. 44, no. 7, pp. 1859–1866, Jul. 2008.

[28] F. Sharifi, M. Mirzaei, B. W. Gordon, and Y. M. Zhang, "Fault tolerant control of a quadrotor UAV using sliding mode control," in *Proc. Conf. on Control and Fault-Tolerant Syst.*, pp. 239–244, Oct. 2010.

[29] Q. Hu and B. Xiao, "Fault-tolerant sliding mode attitude control for flexible spacecraft under loss of actuator effectiveness," *Nonlinear Dynam.*, vol. 64, no. 1-2, pp. 13–23, Apr. 2011.

[30] B. Xiao, Q. Hu, and Y. M. Zhang, "Adaptive sliding mode fault tolerant attitude tracking control for flexible spacecraft under actuator saturation," *IEEE Trans. Control Syst. Technol.*, vol. 20, no. 6, pp. 1605–1612, Nov. 2012.

[31] Q. Hu and B. Xiao, "Adaptive fault tolerant control using integral sliding mode strategy with application to flexible spacecraft," *Int. J. Syst. Sci.*, vol. 44, no. 12, pp. 2273–2286, Dec. 2013.

[32] T. Wang, W. Xie, and Y. M. Zhang, "Sliding mode fault tolerant control dealing with modeling uncertainties and actuator faults," *ISA T.*, vol. 51, no. 3, pp. 386–392, May. 2012.

[33] T. Li, Y. M. Zhang, and B. W. Gordon, "Passive and active nonlinear fault-tolerant control of a quadrotor unmanned aerial vehicle based on the sliding mode control technique," *P. I. Mech. Eng. I-J. Sys.*, vol. 227, no. 1, pp. 12–23, Jan. 2013.

[34] J. P. V. S. Cunha, R. R. Costa, L. Hsu, and T. R. Oliveira, "Output-feedback sliding-mode control for systems subjected to actuator and internal dynamics failures," *IET Control Theory A.*, vol. 9, no. 4, pp. 637–647, Feb. 2015.

[35] Q. Hu, B. Li, and A. Zhang, "Robust finite-time control allocation in spacecraft attitude stabilization under actuator misalignment," *Nonlinear Dynam.*, vol. 73, no. 1-2, pp. 53–71, Jul. 2013.

[36] M. T. Hamayun, C. Edwards, and H. Alwi, "A fault tolerant control allocation scheme with output integral sliding modes," *Automatica*, vol. 49, no. 6, pp. 1830–1837, Jun. 2013.

[37] B. Wang, K. A. Ghamry, and Y. M. Zhang, "Trajectory tracking and attitude control of an unmanned quadrotor helicopter considering actuator dynamics," in *Proc. 35th Chinese Control Conf.*, pp. 10 795–10 800. IEEE, Jul. 2016.

[38] T. Bresciani, "Modelling, identification and control of a quadrotor helicopter," Master's thesis, Lund University, Sweden, 2008. [Online]. Available: http://lup.lub.lu.se/student-papers/record/8847641

[39] M. Wang, J. Yang, G. Qin, and Y. Yan, "Adaptive fault-tolerant control with control allocation for flight systems with severe actuator failures and input saturation," in *Proc. Am. Control Conf.*, pp. 5134–5139. IEEE, Jun. 2013.

[40] V. Utkin and J. Shi, "Integral sliding mode in systems operating under uncertainty conditions," in *Proc. 35th IEEE Conf. on Decis. and Control*, pp. 4591–4596. IEEE, Dec. 1996.

[41] J.-J. Slotine and S. S. Sastry, "Tracking control of non-linear systems using sliding surfaces, with application to robot manipulators," *Int. J. Control*, vol. 38, no. 2, pp. 465–492, Dec. 1983.

[42] J. A. Petersen and M. Bodson, "Constrained quadratic programming techniques for control allocation," *IEEE Trans. Control Syst. Technol.*, vol. 14, no. 1, pp. 91–98, Jan. 2006.

[43] S. Ding, *Model-based fault diagnosis techniques: design schemes, algorithms, and tools*. Springer Science & Business Media, 2008.

Ban Wang received his B.S. and M.S. degrees from Northwestern Polytechnical University, Xi'an, China, in 2011 and 2014, respectively. He is currently pursuing the Ph.D. degree in mechanical engineering with the Department of Mechanical, Industrial & Aerospace Engineering, Concordia University, Montreal, Canada.

His current research interests include fault detection and diagnosis and fault-tolerant control with applications to aircraft and unmanned aerial vehicles.

Youmin Zhang (M'99-SM'07) received his B.S., M.S., and Ph.D. degrees from Northwestern Polytechnical University with specialization in automatic controls, Xi'an, China, in 1983, 1986, and 1995, respectively. He is currently a Professor at the Department of Mechanical, Industrial & Aerospace Engineering and the Concordia Institute of Aerospace Design and Innovation (CIADI), Concordia University, Montreal, Canada.

His current research interests include fault diagnosis and fault-tolerant (flight) control systems, cooperative GNC of unmanned aerial/space/ground/surface vehicles. He has authored four books, over 450 journal and conference papers, and book chapters.

Dr. Zhang is a Fellow of CSME, a Senior Member of AIAA and IEEE, Vice-President of International Society of Intelligent Unmanned Systems, and a member of the Technical Committee for several scientific societies. He is an Editorial Board Member, Editor-in-Chief, Editor-at-Large, Editor or Associate Editor of several international journals. He has served as the General Chair, the Program Chair, and IPC Member of several international conferences.